J. Fluid Mech. (1970), *vol.* 43, *part* 1, *pp.* 145–164
Printed in Great Britain

Experimental investigations of the stability of channel flows. Part 1. Flow of a single liquid in a rectangular channel

By TIMOTHY W. KAO AND C. PARK

Department of Space Science and Applied Physics,
The Catholic University of America, Washington, D.C. 20017

(Received 22 September 1969)

The stability of the laminar flow in a rectangular channel with aspect ratio 1:8 was investigated experimentally, with and without artificial excitation. The critical Reynolds number based on the hydraulic diameter and the average velocity was found to be 2600. Behaviour of damped and growing waves, using artificial excitation, was examined in detail. In particular the progress of growing disturbances was followed. Breaking was found to be the ultimate fate of a growing wave. Spectra of growing and damped waves were also obtained. Measurements were made for wavelengths, wave speeds and amplification or damping rates. The neutral stability boundary in the α_r, R plane was determined. In the damped region, comparison of several aspects of the behaviour of the measured disturbances with the plane Poiseuille theory for spatial decay yielded good agreement.

Three-dimensionality and non-linear subcritical instability were briefly examined. Neutral subcritical waves at low Reynolds numbers appeared possible when the exciter amplitude was quadrupled.

The possible bearings of the present study on the stability of plane Poiseuille flow are suggested.

1. Introduction

The present experimental investigation started with the intention of studying the stability of co-current flow between parallel walls of two immiscible liquids such as oil and water. Such problems are of interest not only for their practical importance but also because they involve two strongly coupled fluids of different densities and viscosities, with a distinct interface separating the two fluids. Furthermore, interfacial waves, which have some resemblance to wind-generated waves have been observed (Charles & Lilleleht 1965). The nature of the stability problem here is a rather complex one. To make a systematic study of the factors involved and to examine the various aspects of the mechanism whereby instability and interfacial wave generation can be accomplished, observations restricted to the interface are insufficient. Mean flow profiles, amplitude distribution of the disturbances, and controlled excitation are needed. Preliminary experiments were performed by Kao & Park (1967) but without controlled excitation so that the results were not sufficiently detailed. Part 2 of this paper will report fully the two-

fluid problem which is now in progress. Here we present the results in the same channel with water alone. This part was undertaken at first merely to obtain the stability characteristics for comparison with the two-layer case, but it was soon realized that this was a major undertaking by itself and the results are of definite interest *per se*.

Since Tollmien–Schlichting waves were first discovered experimentally by Schubauer & Skramstad (1948) the techniques of using artificial disturbances for mapping out stability boundaries that they employed have been successfully used in a variety of experiments on flow stability. Most of the experiments were done for nearly parallel flow in which the Reynolds number changes with downstream distance. For strictly parallel flows in pipes or channels, we found that controlled experimental results on stability are scanty indeed. Leite (1959) gave a well-documented set of experimental results for the circular pipe flow. In that case, small disturbances are always damped, so that only damped disturbances were discussed by Leite. As for the stability of plane Poiseuille flow and rectangular channel flow, no controlled experimental results are available at all. There only exists several sets of hydraulic experiments where transition was estimated by measuring the head losses. Schiller (1923) found critical Reynolds numbers of 1000 and 1600 based on the hydraulic diameter using a square and a rectangular channel with aspect ratio 1:3·5 respectively. Davis & White (1928), using a 'built-up' rectangular channel 2·54 cm in breadth and of variable depth from 0·015 cm to 0·068 cm (aspect ratios ranging from 1:710 to 1:38) found critical Reynolds numbers based on the depth ranging from 890 to 355 respectively. Unfortunately, these experiments were based solely on measuring head losses and there is thus no way to evaluate the results properly. Suffice it to say that the critical Reynolds numbers found by Davis & White (1928) were unusually low. It was sometimes thought (Reynolds & Potter 1967) that the low values of Davis & White were due to non-linear subcritical instability, because the depth was so small.

Compared with the experimental stability study of boundary-layer, free shear layer, two-dimensional jets and wakes, controlled measurements of stability in pipes and channels have additional difficulties. As one now works with smaller cross-sections and leakage has to be prevented, the use of easily movable carriages for probing the flow at many locations is hindered. In our experiment a channel with a cross-section $H \times 2b = 1\text{ in.} \times 8\text{ in.}$ was used. Aspect ratio is defined as 1:half-width of channel/half-depth of channel which is $1:b/h$ ($= 1:8$ in the present case). It is said to be large when b/h is large. With this aspect ratio there is theoretically a mid-section 4 in. wide in which the mean flow is uniform spanwise to within 0·175 % and the profile across the depth is plane Poiseuille to the same order of accuracy. Rectangular channel flows are, to be sure, different from plane Poiseuille flow as far as stability is concerned, except when the aspect ratio is very large, say, of the order of $1:10^2$ as in Davis & White (1928). However, a section of depth sufficient for detailed measurements but with such large aspect ratios was unfeasible with our facilities. We are therefore only concerned with rectangular channel flow, although the results here may have some bearing on the plane Poiseuille problem.

In this paper we present the experimentally determined neutral stability curve

for the rectangular channel and the nature of damped and growing disturbances together with some results on the mechanism of transition. Water was used as the working fluid because the next experiment, to be reported in part 2, is designed for a study of oil and water.

Comparison of the measurements in the damped region with the plane Poiseuille theory for spatial decay is made. (We owe the theoretical results to Professor W. C. Reynolds of Stanford University who kindly furnished us with his computer results.) Good agreement is found with that theory in several aspects.

2. Experimental set-up and procedure

The plan of the laboratory set-up is shown in figure 1. The plexiglass channel (cross-section 1 in. × 8 in.) is a re-circulating type. The flow was maintained by a constant head tank which was provided with a continuously adjustable overflow device, and was discharged into a downstream control tank. The discharged water was continuously by-passed to give a constant temperature and greater purity to the water in the system. A highly steady condition in the flow-rate as well as in the temperature was achieved. An on-line filter capable of filtering the water down to 40 μ was installed to ensure water purity. Temperature was monitored by thermometers at different points in the system. Two flow-rate meters (Fisher and Porter, model no. 10A2700) were installed in parallel ahead of the inlet section to the channel, and the rate of discharge through the channel could be read directly. In the inlet section turbulence was suppressed through a section packed with plastic drinking straws $1\frac{1}{2}$ mm in diameter, and bounded on each side by a fine-mesh screen, followed by a series of three additional fine-mesh screens, before entering the channel.

Measurements of the mean flow profile and disturbances were made by means of hot-film anemometers. Miniature probes (model 1270-10W-6, Thermosystems, Inc.) with hot-film quartz-coated sensors (0·001 in. diameter and 0·020 in. long on a glass cylinder 0·001 in. diameter and 0·050 in. long) were used. The prongs of the probes were gold coated and 0·25 in. long and the stainless steel stem was 0·059 in. in diameter and 6 in. long. Two channels of hot-film anemometers were used. Recording was done conveniently on a dual-channel Sanborn chart recorder which was found to be very good for low frequency work. Calibration of the hot-films was done by towing the probes in a separate flume 10 ft. long and 4 in. wide using a variable speed motor. The probe support assemblage was mounted on a sliding plate (figure 2(*a* ii) and 2(*c*)) which could then be moved along the length of the channel with the vertical position adjustable to within 0·001 in. by means of a micrometer. The assemblage could also be attached to the main channel at various fixed positions of probe insertion points. In all cases, the sensing cylinder was placed normal to the direction of flow so that the velocity was measured along the X-direction, where X is the horizontal distance along the length of the channel measured downstream from the ribbon, Y is the vertical distance through the depth of the channel measured from the bottom and Z is the horizontal distance across the width of the channel measured from the spanwise centreline.

The disturbance generator was an important part of the experimental set-up.

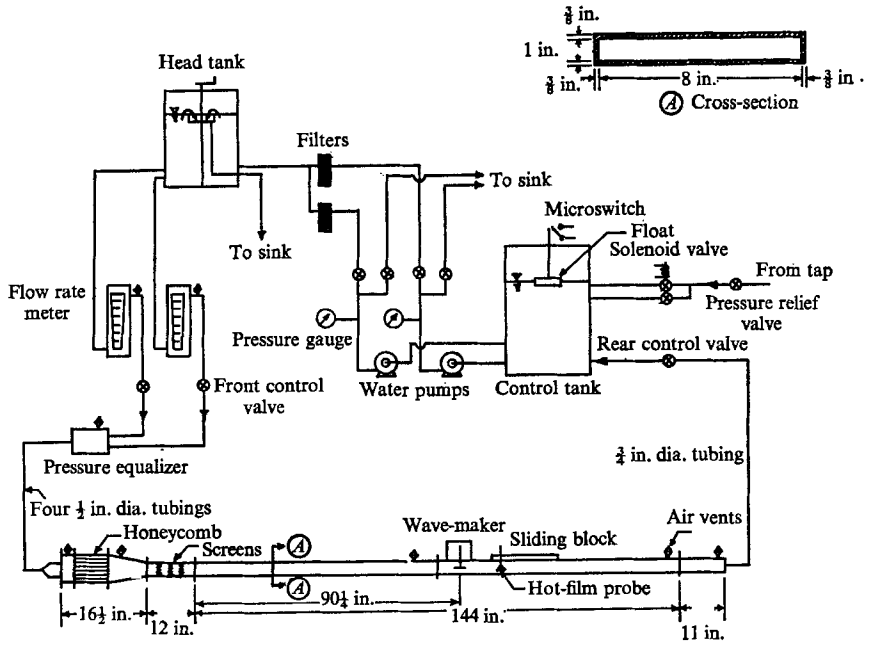

FIGURE 1. Plan of laboratory set-up.

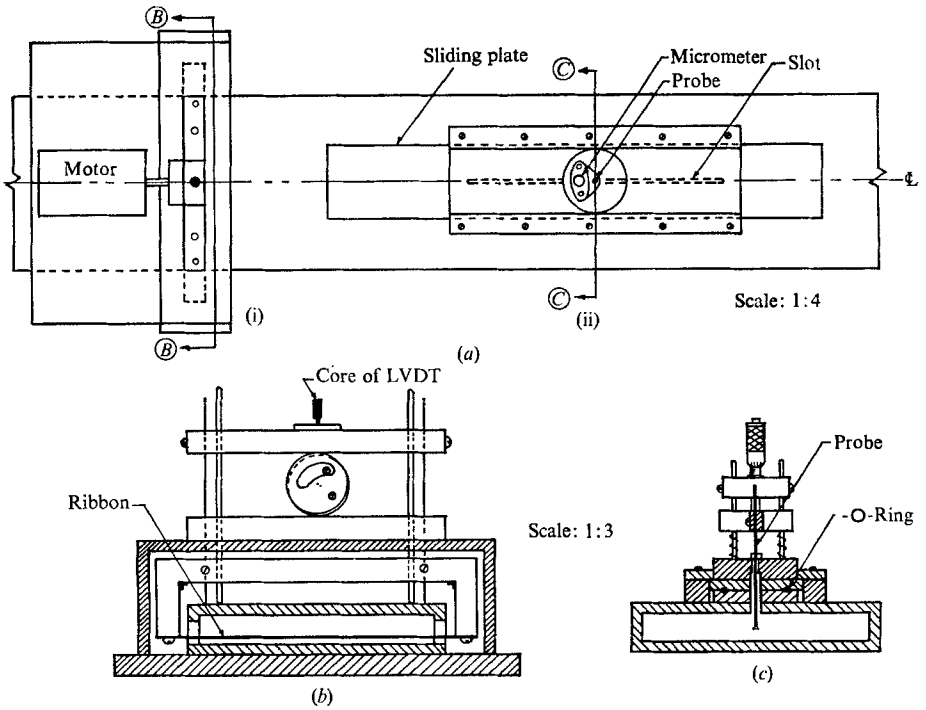

FIGURE 2. (*a*) Plan view of channel with wave generator at (i) and sliding mount and probe assemblage at (ii). (*b*) Sectional view of wave generator, section *B–B*. (*c*) Sectional view of sliding mount with probe assemblage, section *C–C*.

A mechanically-driven exciter was constructed, capable of generating sinusoidal disturbances in a frequency range of $\frac{1}{20}$ to 50 c/s with the aid of a synchronous d.c. servomotor. (This was preferred to electromagnetic driving which was unsatisfactory for low frequencies.) The wave-making part was a thin stainless steel ribbon 0·001 in. thick and $\frac{1}{4}$ in. wide extending across the entire width of the channel and placed near the bottom wall, at 0·075 in. from it for the small disturbances of §3 and at 0·175 in. for the large amplitude disturbances of §4. The amplitude of the wave-maker could be adjusted to any desired magnitude so that linear as well as non-linear effects could be studied. The input signal to the fluid from the wave-maker was monitored through a linear variable differential transformer (LVDT) and the signal was recorded on the Sanborn recorder. The disturbance generator assemblage is shown in figure 2(*a* i) and 2(*b*).

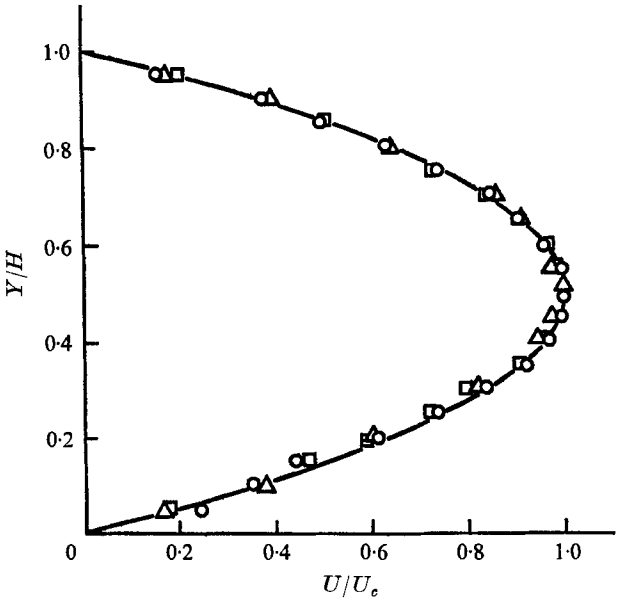

FIGURE 3. Mean flow profiles, ○, $R = 1320$ at $X = 13$ in.; □, $R = 900$ at $X = -26{\cdot}5$ in.; △, $R = 1150$ at $X = -26{\cdot}5$ in.

For each experiment, the channel was first thoroughly cleaned. It was then filled and pressurized and any air bubble was removed and leakages were checked. The system was then allowed to run for a few minutes until steady flow and temperature conditions were established.

Mean flow profiles were measured for a large number of flow rates and at different positions along the length of the channel. Some typical ones are shown in non-dimensional form in figure 3. In all cases the data were taken at stations where the flow was estimated to be fully developed. Measurements were also taken with and without the non-operating wave-maker in place. No detectable difference on the mean flow was found. In measuring the mean flow the probe was calibrated before and after each test. Measurements proceeded from the top to the bottom and were repeated from the bottom to the top for the same vertical positions. The two sets were then averaged to cancel any positional and

wall-effect errors. The results of the mean flow were checked *in situ* by timing a dye-trace released at mid-depth, as well as comparing with the flow rate reading. Good agreement of these three independent methods was obtained for the centre-line velocity. Good agreement with the theoretical plane Poiseuille profile was also obtained as shown in figure 3. The mean flow profile for a rectangular channel can be easily calculated and was first given by Cornish (1928). For a channel with aspect ratio 1:8 the result shows that the centre 4 in. spanwise is flat. This was tested by observing dye lines released simultaneously at mid-depth and each at $1\frac{3}{4}$ in. apart from the spanwise centreline. The velocities were found to be indeed the same as that at the spanwise centreline at mid-depth.

The experimental procedure for the flow with artificial excitations was as follows. For each experiment a steady flow was first achieved as described previously. The temperature and flow-rate were read to give the Reynolds number of the flow. The mean flow was checked with the hot-film for steadiness. In the fully laminar range no residual fluctuations were detectable with the exciter off. The exciter was then turned on and operated at different frequencies, and damped disturbances were investigated. The disturbances were surveyed by the hot-film depthwise and longitudinally downstream of the ribbon from $X = 13$ in. to $X = 20{\cdot}5$ in. along the spanwise centreline ($Z = 0$). Such experiments were done for increasing Reynolds numbers, R, based on the hydraulic diameter $d(= 4A/p$, A = cross sectioned area, p = peripheral length of cross-section) and average flow velocity $U_m\,(= Q/A$, Q = flow rate). In the range where the flow began to be unstable, natural disturbances appeared in turbulent spots or eddies with the exciter off. The same procedure was adopted as for the damped region.

For phase comparisons, one hot-film probe was held stationary with the other moved relative to it either depthwise or longitudinal-wise. Wavelengths (λ) were measured, with two sensors at the same vertical level, by displacing one probe longitudinally downstream until the phase had increased by 360° as measured on the simultaneous recording of the signals on the Sanborn recorder. The wave speed was then calculated from the known frequency (f) by the formula $c = \lambda f$. To avoid any interference from the first probe the second probe was inserted from the opposite side. Wave speed could also be measured with one probe by switching the oscillator off and timing the arrival of a phase point of the last wave and then switching the oscillator on again and timing the arrival of a phase point of the first wave, using the signal from the LVDT as reference. Knowing the distance of the probe from the oscillator and knowing the average time for the wave to travel this distance, the wave speed was calculated. It was found that the two methods agree to within 10%, which was in the range of accuracy of the first method. The second method was thus widely used for rapid reading and in the higher Reynolds number range.

Since no commercial filter or spectrum analyzer works satisfactorily at these very low frequencies, parts of the recorded signals were later digitized and then Fourier analyzed on a computer (IBM 1130) for spectral components. 98 sets of spectra were obtained in this manner, a few representative samples of which will be reproduced in this paper.

The temperature range of the experiments was from 51 to 80 °F.

3. Measurements of disturbances and stability boundary

Experiments were first carried out without excitation for a range of Reynolds numbers. For Reynolds numbers up to 2500 the flow was laminar. A typical hot-film output at this Reynolds number is shown in figure 4 (*a*). (The time scale for this record is 5 times that shown which is at 1 sec intervals, so that this strip covers a time span of 193 sec.) The residual motion is here less than 0·01 per cent, and was much less at lower Reynolds numbers. As the Reynolds number was increased, turbulent bursts or eddies began to appear. A typical bursting is shown in figure 4 (*b*) for a Reynolds number of 3050. Further increase in Reynolds number caused an increase in the intensity and frequency of bursts as shown in figure 4 (*c*).

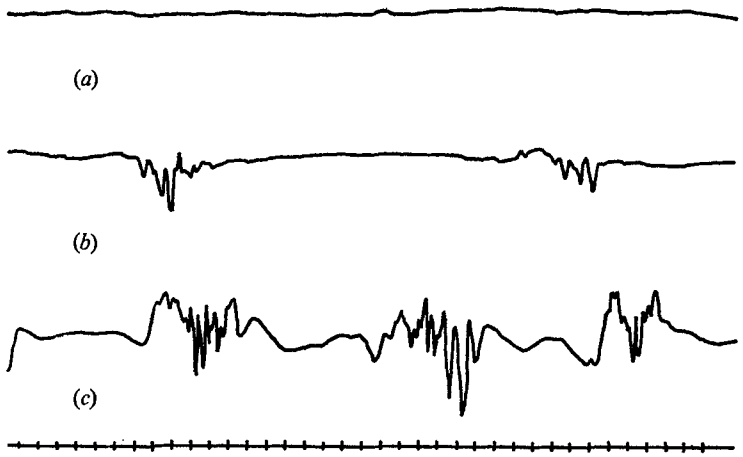

FIGURE 4. Natural disturbances: (*a*) at $R = 2500$, (*b*) at $R = 3050$, (*c*) at $R = 3280$. Time between marks at bottom is 1 sec.

The major effort of the investigation was to examine the nature and behaviour of sinusoidal disturbances introduced at different frequencies by means of the vibrating ribbon. The position of the ribbon was at 0·075 in. from the bottom wall. It was found that an amplitude of 0·02 in. maximum displacement was satisfactory for the range of frequencies and Reynolds numbers explored.

Figure 5 shows the amplitude distributions of u'/U_c, where u' is the root-mean-square value of u, the instantaneous X component of fluctuation velocity, and U_c is the velocity at the centre of the channel cross-section ($= 0{\cdot}7836\,Q$), across the depth of the channel for several distances downstream for a typical damped disturbance at low Reynolds numbers ($R = 1350, f = 0{\cdot}444$ Hz). They are nearly symmetric with maximum peak remaining essentially at a constant location with distance downstream. A second smaller peak is often present. The maximum value of u'/U_c is about 0·7 %. A large number of experiments were done in the damped region with similar results.

Figure 6 shows the simultaneous recording of two hot-film output signals at $X = 13{\cdot}5$ in. for a damped mode at $R = 2740, f = 0{\cdot}445$ Hz. The lower trace is from a hot-film fixed at $Y = 0{\cdot}05$ in. from the bottom wall and the upper trace

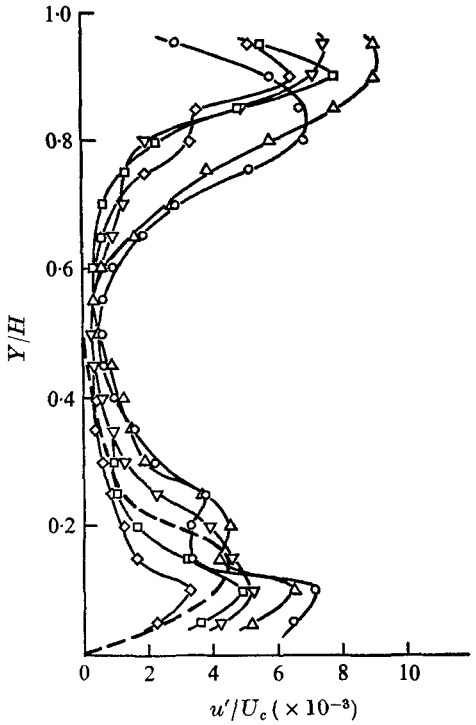

FIGURE 5. Vertical distributions of amplitude with distance downstream, $R = 1350$, $f = 0{\cdot}444$ Hz. ○, $X = 13$ in.; △, $X = 15$ in.; ▽, $X = 17$ in.; □, $X = 19$ in.; ◇, $X = 20{\cdot}5$ in. ————, theoretical curve from the spatial problem of the plane Poisuille theory as calculated by Reynolds.

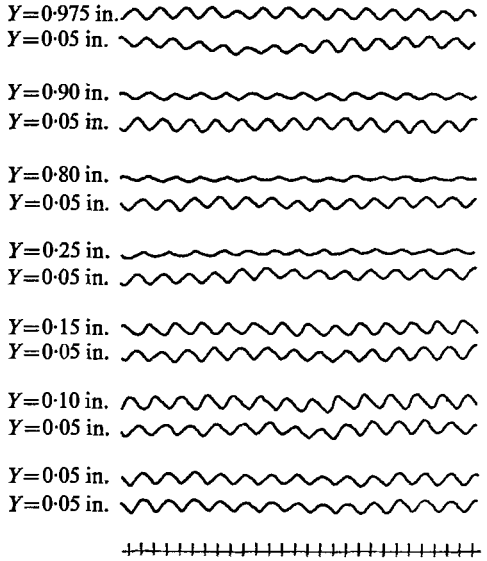

FIGURE 6. Simultaneous recording showing amplitude and phase difference of two hot-film output signals at $X = 13{\cdot}5$ in., for a damped mode at $R = 2740, f = 0{\cdot}445$ Hz. The lower trace is fixed at $Y = 0{\cdot}05$ in. while the upper trace is at different Y's. Time between marks at bottom is 1 sec.

is from a hot-film, which was moved vertically across the depth of the channel as indicated in the figure. The signals are very pure and sinusoidal. Notice that a 180° phase shift has occurred between $Y = 0{\cdot}10$ in. to $Y = 0{\cdot}20$ in. The wave velocity was measured to be 2·27 in./sec. and the centreline velocity was 3·52 in./sec. Thus the point Y_c at which the flow velocity equalled the wave velocity was at $Y = 0{\cdot}19$ in. The phase shift therefore has occurred around the critical layer. A second change in phase near the top was however not observed although the amplitude distribution across the depth is reasonably symmetric.

Figure 7 shows the damping downstream of a damped disturbance at $R = 2720$ and $f = 0{\cdot}667$ Hz. The lowest trace shown is the input signal given by the LVDT. The next three traces up are the hot-film outputs at $Y = 0{\cdot}1$ in. and $X = 13$ in., 17 in. and 20·5 in. respectively. The wavelength was measured to be 3·36 in. and

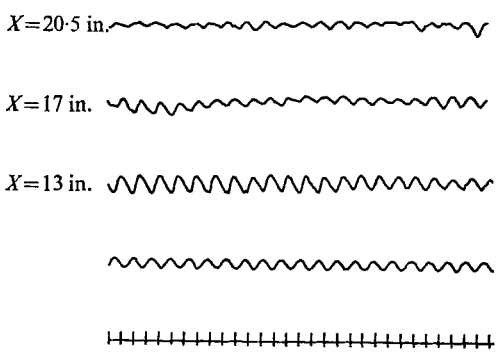

FIGURE 7. Hot-film outputs for a damped disturbance at $Y = 0{\cdot}1$ in. and $X = 13$ in., 17 in., 20·5 in. $R = 2720$, $f = 0{\cdot}667$ Hz. Lowest trace is signal from LVDT. Time between marks at bottom is 1 sec.

the wave-speed was 2·24 in./sec. (The traces are here displayed without regard to phase relationships.) The output signals were Fourier analyzed and the spectra for these three positions are shown in figure 8. The maximum amplitude was about 2 % of U_c at $X = 13$ in. We observe that only a weak harmonic is present so that the wave is linear in this range. This fact is further confirmed by plotting $\log_{10}(u'/u'_0)$ against $(X - X_0)/h$, where u'_0 is value of u' at $X = X_0 = 13$ in. This is seen to be a straight line as shown in figure 12, so that the wave is exponentially damped as required by the linear theory.

The previous illustrations of the nature of damped disturbance are typical ones. The damped disturbances are thus well behaved for the whole range of Reynolds numbers tested.

At Reynolds numbers higher than 2600 both damped and growing disturbances were found. A typical growing disturbance is shown in figure 9 for $R = 2710$ and $f = 1{\cdot}05$ Hz. Again the lowest trace shows the input signal given by the LVDT, and the next three traces up show the hot-film outputs at $Y = 0{\cdot}1$ in. and $X = 13$ in., 17 in. and 20 in. respectively. The maximum amplitude of the disturbance is about 4 % (with a smaller r.m.s. value) of U_c at $X = 13$ in. and has more than doubled at $X = 20$ in. A higher harmonic indicative of breaking is beginning to appear on the uppermost trace. The linearity limit at this Reynolds

number is about 8 % of U_c. We also note the presence of a very low frequency oscillation, perhaps indicating a large-scale three-dimensional effect. Figure 10 shows a typical breaking wave ($R = 2720$ and $f = 0{\cdot}87$ Hz). The arrangement of the traces is the same as the last one. Here one notices a large eddy on the trace

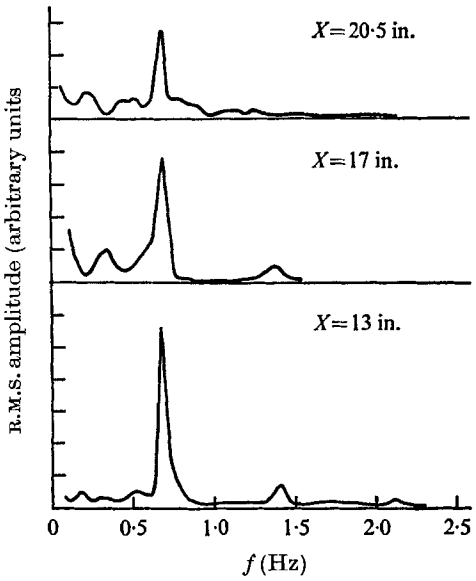

FIGURE 8. Spectra for the damped disturbance at $Y = 0.1$ in. and $X = 13$ in., 17 in., 20·5 in. $R = 2720, f = 0{\cdot}667$ Hz.

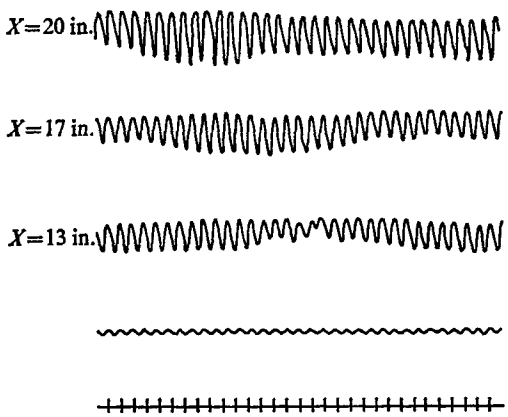

FIGURE 9. Hot-film outputs for a growing disturbance at $Y = 0{\cdot}1$ in. and $X = 13$ in., 17 in., 20 in. $R = 2710$, $f = 1{\cdot}05$ Hz. Lowest trace is signal from LVDT. Time between marks at bottom is 1 sec.

at $X = 13$ in. The growth rate is very rapid, and at $X = 17$ in., where the maximum amplitude has reached about 8 % of U_c, the wave shows incipient breaking with the appearance of one dominant higher harmonic. In the top trace at $X = 20{\cdot}5$ in., a larger number of frequencies are now present indicating breaking of the wave.

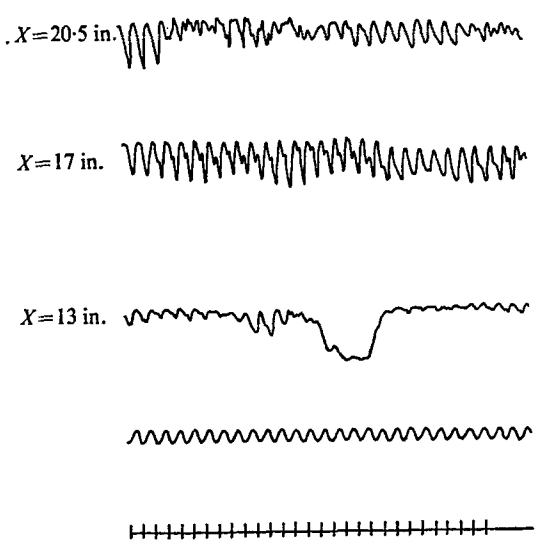

FIGURE 10. Hot-film outputs for a breaking disturbance at $Y = 1{\cdot}0$ in. and $X = 13$ in., 17 in., 20·5 in. $R = 2720$, $f = 0{\cdot}87$ Hz. Lowest trace is signal from LVDT. Time between marks at bottom is 1 sec.

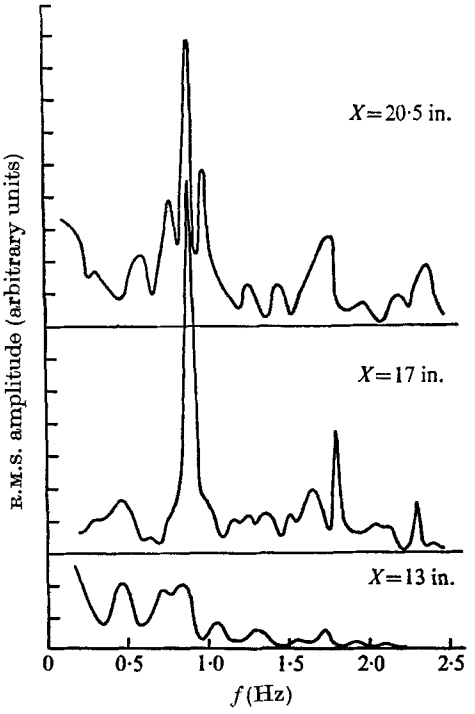

FIGURE 11. Spectra for the breaking disturbance at $Y = 0{\cdot}1$ in. and $X = 13$ in., 17 in., 20·5 in. $R = 2720$, $f = 0{\cdot}87$ Hz.

The spectra at these positions are shown in figure 11. A minor peak of about one half the frequency of the dominant is present, probably from existing natural disturbances, and is not appreciably affected by the wave-breaking process. The spectra also has a very low frequency tail. Notice the richer frequency content of the spectrum at $X = 20$ in. after wave-breaking has occurred.

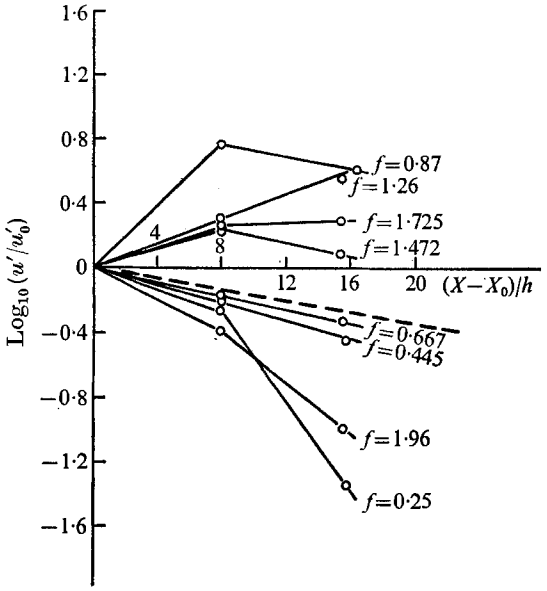

FIGURE 12. Decay and growth of u' component of disturbances, $R = 2720$. ———, theoretically calculated damping rate for $f = 0{\cdot}445$ as given by Reynolds.

Figure 12 shows the typical decay and growth behaviour at a fixed Reynolds number for various frequencies, measured at $Y = 0{\cdot}1$ in. from $X_0 = 13$ in. by plotting $\log_{10}(u'/u'_0)$ against $(X - X_0)/h$. The result shows that while most damped disturbances decay exponentially, the growing ones are somewhat less well behaved. (It should be borne in mind that, due to the leakage-proof requirement on the sliding mount and the disturbance generator, measurements started at 13 in. downstream from the ribbon, which was several wavelengths away. The linearity of the disturbances was thus very well preserved over such a large distance.) It was found that whenever there was a rapid growth, wave-breaking inevitably resulted as in the case of $R = 2720$, $f = 0{\cdot}87$ Hz included in figure 12. This sort of behaviour was very typical and occurred in many instances.

The spectrum of an exponentially growing mode ($R = 2720$, $f = 1{\cdot}25$ Hz) is shown in figure 13. Some non-linearity is beginning to make its appearance at $X = 20$ in. with a sizable first harmonic. Figure 14 shows the vertical structure of a growing mode ($R = 3040$, $f = 0{\cdot}67$ Hz). The various interesting shapes of the disturbance at different vertical locations may perhaps be attributable to the arrangement and details of the eddies generated by the ribbon. (In the damped cases these details were apparently smoothed out in about a few wavelengths.) In particular, unlike the boundary-layer case studied by Klebanoff & Tidstrom (1959), the 'hairpin'-like signal at mid-depth is not an indication of

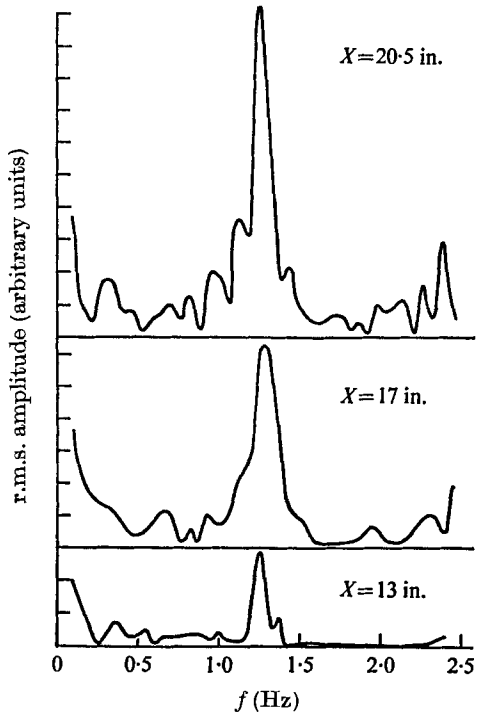

FIGURE 13. Spectra for a growing disturbance, at $Y = 0{\cdot}1$ in. and $X = 13$ in., 17 in., 20·5 in. $R = 2720, f = 1.25$ Hz.

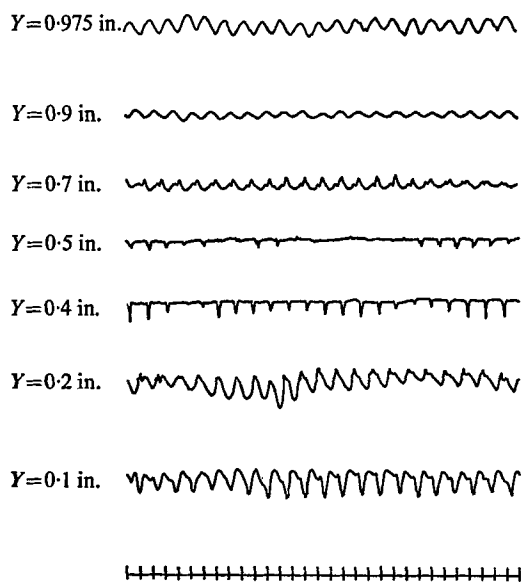

FIGURE 14. Shapes of a growing disturbance at different vertical positions $R = 3040, f = 0{\cdot}67$ Hz.

where breakdown occurs. This shape was found to be preserved and amplified as the disturbance travelled downstream without generation of higher frequencies at the 'hairpin' end.

At higher Reynolds numbers, in order to examine the behaviour of a wave at a fixed frequency when the flow was excited at that frequency, the output from the hot-film should be filtered, since the natural flow has an abundance of disturbances. This was accomplished by recording the complete output and Fourier analyzing the data as before. This entailed a great amount of work. The natural disturbances of the type shown in figure 4 were also Fourier analyzed. The spectral contents were found to be compatible with the frequency range of the growing modes found with artificial excitation.

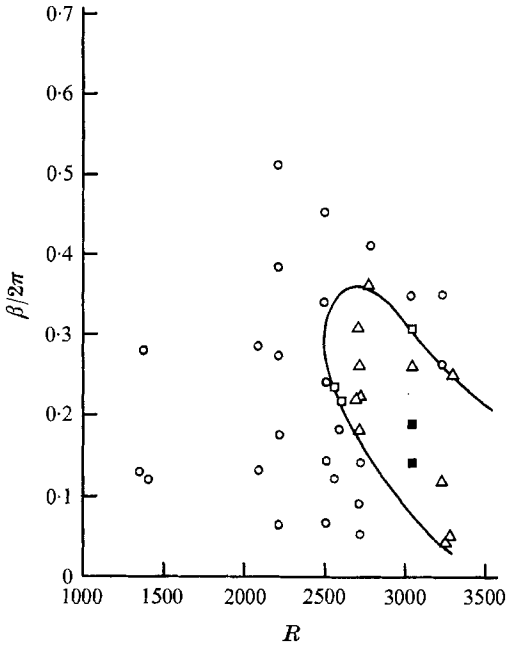

FIGURE 15. β, R plane showing regions of damping and growing and neutral stability boundary. ○, damped; △, growing; □, neutral; ■, growing but less certain.

A large number of experiments were carried out over a range of frequencies and Reynolds numbers, the growth or decay and the wave speed were determined for each case. These are summarized on a frequency parameter Reynolds number plot as shown in figure 15. The plot exhibits a growing and a damped region which can be separated by a neutral stability boundary. The critical Reynolds number is 2600, in good agreement with the result of natural instability without artificial excitations. Another useful plot is shown in figure 16 where the dimensionless wave-speed c/U_m is plotted against R. Again the growing region can be separated from the damped region by a stability boundary. Notice that the mean velocity has been used for non-dimensionalizing the wave velocity. From the above two graphs we may finally obtain an α_r, R plot ($\alpha_r = 2\pi h/\lambda$, dimensionless

wave-number). This is shown in figure 17. The least stable mode is at $\alpha_r = 1{\cdot}5$ and $R = 2600$.

Table 1 lists the wavelength λ, wave-number α_r, non-dimensional frequency $\beta(= 2\pi fh/U_m)$, and the amplification coefficient $-\alpha_i$ for points around the neutral

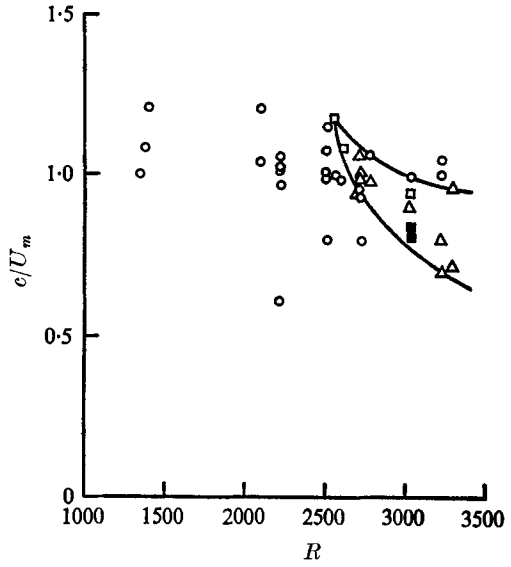

FIGURE 16. (c/U_m), R plane showing regions of damping and growing and neutral stability boundary. ○, damped; △, growing; □, neutral, ■, growing but less certain.

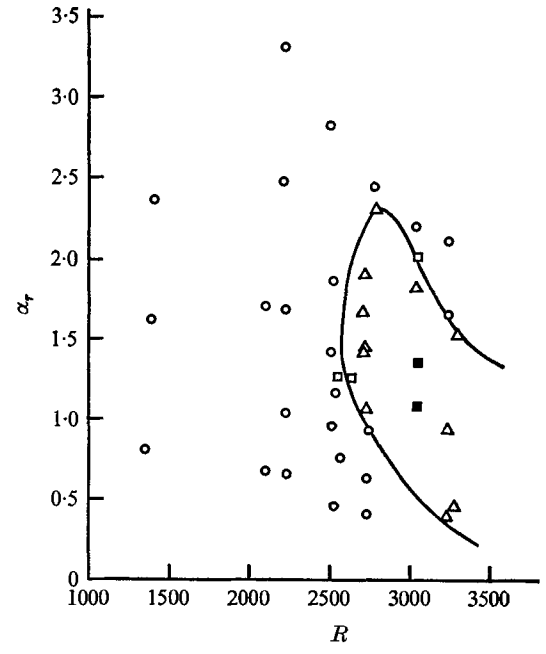

FIGURE 17. α_r, R plane showing regions of damping and growing and neutral stability boundary. ○, damped; △, growing; □, neutral; ■, growing but less certain.

stability curve on both sides of the critical Reynolds number. The values of α_i are calculated from

$$\alpha_i = -2{\cdot}3\frac{d}{dx}\left(\log_{10}\frac{u'}{u'_0}\right),$$

where $x = X/h$. The results of α_i further confirm the consistency of the data. In general, with one or two exceptions, the damping or growing rate is larger as a point moves farther away from the neutral stability curve.

Since the experiment was set up to study the spatial decay or growth of disturbances, the data are therefore presented accordingly; i.e. in the normal mode decomposition the wave-number α is complex and the frequency parameter β is real in the factor $\exp\{i(\alpha x - \beta t)\}$ where t is the dimensionless time normalized

R	Wavelength λ	Dimensionless wave-number, α_r	Frequency parameter, β	Amplification factor, $-\alpha_i$
2570	4·07	0·77	0·779	−0·1190
2510	3·23	0·972	0·911	−0·0609
2550	2·68	1·172	1·150	−0·0241
2510	2·21	1·421	1·521	−0·0564
2510	1·685	1·870	2·130	−0·0462
2610	2·48	1·265	1·360	0·1501
2720	7·54	0·416	0·330	−0·1920
2720	5·10	0·614	0·587	−0·0646
2720	3·36	0·935	0·880	−0·0477
2720	2·92	1·705	1·150	0·2225
2710	2·19	1·435	1·389	0·1165
2720	2·13	1·475	1·389	0·1736
2720	1·88	1·670	1·652	0·0837
2720	1·64	1·915	1·942	0·0192
2720	1·36	2·31	2·268	0·0730
2720	1·29	2·44	2·589	−0·1472

TABLE 1

by h/U_m. For the damped region, a comparison with the Orr–Sommerfeld theory for plane Poiseuille flow is in order. Some calculations for the spatial decay problem of the above theory are made available to us through the courtesy of W. C. Reynolds. The shape of the u' amplitude curve for $R = 1350$ and $f = 0{\cdot}445$ Hz as calculated by Reynolds is sketched by the dotted line in figure 5. It agrees quite well with that measured, especially with regard to the position of maximum amplitude. The calculations for $R = 2740$ and $f = 0{\cdot}445$ Hz showed similar agreement with the measurements in figure 6, although the phase changes in the measurements appeared larger than those in the theoretical calculations and the mode is neither symmetric nor quite antisymmetric. The theoretically predicted spatial decay for this case was also computed by Reynolds and this is shown by the dotted line on figure 12. One notes that the agreement with the measured decay is good. The results therefore indicate that in the damped region the disturbances behave much like disturbances in the plane Poiseuille case.

We note here that in any experiment using an exciter of fixed frequency, it is possible that a number of modes of different wave-numbers are excited at a given Reynolds number. Gill (1965) has shown that the use of more than one mode (two, for example) is often sufficient to account for, more precisely, the shape of the amplitude distribution and the phase changes in Leite's (1959) experimental study of the circular pipe flow case. A similar calculation may also improve the agreement between the predicted and measured phase changes in the present case.

4. Three-dimensional and non-linear effects

Limited experimentation was carried out on three-dimensional and non-linear effects. The presence of the lateral boundaries and the fact that the wavelengths measured were comparable with the lateral dimension indicate that the disturbances must be three-dimensional. The exploration of the spanwise structure would be desirable. However, difficulty in constructing a leak-proof spanwise traverse mechanism prevented a detailed study of the three-dimensional nature of the waves. Since the disturbances were mostly in the linear range, the details of three-dimensionality may not be too important as was suggested in previous studies. The disturbances in Schubauer & Skramstad's (1948) experiments were, for example, three-dimensional in the linear range as demonstrated later by Klebanoff & Tidstrom (1959); and according to Klebanoff, Tidstrom & Sargent (1962), the results were still in excellent agreement with the Tollmien–Schlichting theory as far as several wavelengths downstream from the ribbon, where the disturbances were strongly three-dimensional. We note also that there was considerable azimuthal dependence for the damped 'axisymmetric' disturbances studied by Leite (1959). Nevertheless, in our investigation, an attempt was made to study three-dimensionality first by flow visualization through dye injection and subsequently by placing a probe at $Z = -1{\cdot}0$ in. It was observed that the disturbance was shed essentially two-dimensionally for the mid-4 in. spanwise of the channel for a distance of about one wavelength and subsequently the motion was three-dimensional with spanwise oscillations developing further downstream away from the spanwise centreline, especially for growing waves. Measurements were made at $X = 13$ in. for a long damped wave with $\lambda = 7$ in. ($R = 2690$, $f = 0{\cdot}25$ Hz). Two probes, one at $Z = 0$ and one at $Z = -1$ in. were used. The result is shown in figure 18. The waves have exactly the same appearance and magnitude through the depth of the channel but with a small but constant phase difference, indicating that in less than two wavelengths, the wave was beginning to take on a three-dimensional character. We also should point out that the mean flow velocity at these two spanwise points were checked and found to be equal. Measurements at $X = 13$ in. for waves of shorter wavelengths indicated more distortion and three-dimensionality with unequal amplitude for the two points. However, no specific conclusions, aside from the fact that they were three-dimensional could be drawn from these measurements.

The generation of a substantial higher harmonic was the first sign of non-linear effect in growing waves. This was soon followed by breakdown of the wave and an

increase in frequency content of the spectrum. Such was the fate of growing waves. Quite aside from these non-linear manifestations, the amplitude of the exciter was varied during the course of the investigation. No appreciable effect on the neutral stability curve was found by doubling the amplitude of the exciter, although the signal became more noisy. The amplitude was later doubled again. This time the output resembled a typical output of fully turbulent flow for higher frequencies of the exciter. However, these still appeared to decay downstream, although very slowly, for Reynolds number somewhat below critical. No attempt was made to explore this fully. Amplitudes sufficient to cause subcritical instability were not reached. Some experiments were, however, made at low Reynolds number with these amplitudes. A neutrally stable disturbance now appeared

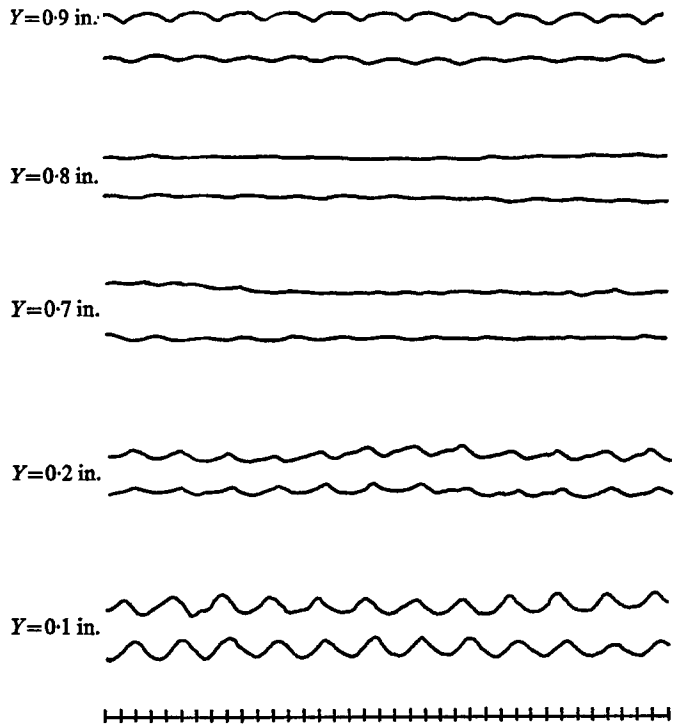

FIGURE 18. Hot-film outputs at $Z = 0$ and $Z = -1$ for various Y's. Lower trace is at $Z = 0$. Upper trace is at $Z = -1$ in. $R = 2690, f = 0{\cdot}25$ Hz.

possible. This is shown in figure 19 for $R = 1660, f = 0{\cdot}67, \lambda = 2{\cdot}12$ in. The amplitude is about 3 % of U_c which is much larger than any damped mode found in this region. At $X = 13$ in. the signal shows the eddy structure, the higher frequencies of which seem smoothed or damped out as the wave travels downstream. Again the arrangement of the traces and the location of the hot-film for these measurements are in the same way as in figure 7. Another such subcritical neutral wave was found at the same frequency but lower Reynolds number ($R = 1440$). It appeared that the threshold amplitude for subcritical instability depended on the Reynolds number as well as the frequency of the disturbance. However, not enough experiments were carried out to warrant any strong conclusions.

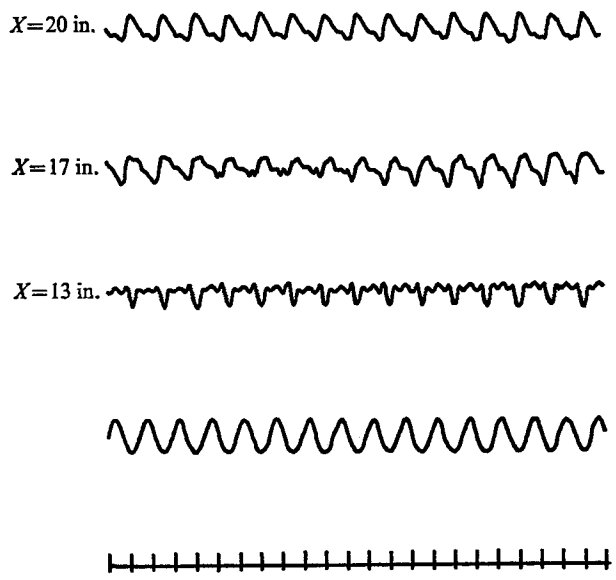

FIGURE 19. Subcritical neutral disturbance at $Y = 0{\cdot}1$ and $X = 13$ in., 17 in., 20 in., with amplitude of exciter quadrupled. $R = 1660, f = 0{\cdot}67$ Hz.

5. Concluding remarks

From the present study, we draw the following conclusions:

(1) A critical Reynolds number, $R = 2600$, was found, below which all small disturbances were damped, and above which there were growing modes. From the controlled experiments, it was possible to obtain a well-defined neutral stability boundary in the α_r, R plane, separating regions of growth and decay. The result of the critical Reynolds number using artificial excitation was in good agreement with the naturally occurring one.

(2) The nature of the damped waves showed a great deal of resemblance to the theoretical predictions for damped disturbances in plane Poiseuille flows, even though the disturbances assumed three-dimensionality in the experiments.

(3) For a fixed Reynolds number above the critical, the growth rate was found to depend on the frequency. The progress of a growing disturbance was followed. Breakdown of a growing wave was found to occur in the form of a sudden, simultaneous increase of various frequencies with a decrease in the amplitude of the dominant.

(4) Subcritical neutral disturbances were present when the oscillating ribbon executed large amplitude motions. The threshold amplitude for these disturbances appeared to depend on Reynolds number and frequency.

On comparing the critical Reynolds number found herein with the theoretical value for plane Poiseuille flow (see, for example, Lin 1955) it is observed that the number here is lower although of the same order. On the other hand the present number is higher than those found by Schiller (1923) for smaller aspect ratios. It is suggested from these results, as well as the results of Davis & White (1928), that

the critical Reynolds number for rectangular channels varies with the aspect ratio, being larger at larger aspect ratio and approaches the plane Poiseuille value when the aspect ratio becomes very large. It is further suggested that the nature of the disturbances, the mechanism of breakdown and transition to turbulence found here in the rectangular channel are similar to those in the plane Poiseuille case. It is our opinion that the presence of the side walls in a rectangular channel, which introduces spanwise variation in the disturbance, enhances energy transfer from the mean flow to the disturbances, thus rendering the flow more unstable than the plane Poiseuille case. The fact that the side walls affect the shape of the mean flow profile also has bearing on the stability problem. On the other hand, when the aspect ratio is large, the stability characteristics of a rectangular channel should be the same as those of the plane Poiseuille case. Clearly any further controlled experiments with smaller or larger aspect ratios would be most useful for giving more susbtance to the suggestions above.

The authors are indebted to Professor W. C. Reynolds of Stanford University, who served as a referee to this paper and kindly made available to us his computer results on the spatial decay problem. We also wish to thank Messrs Michael McGrath and Michael McGlynn for their help in the experiments, and particularly for the task of reducing the analogue data to digital form.

The authors are also grateful to the National Science Foundation for their support under grant GK-2639.

REFERENCES

Charles, M. E. & Lilleleht, L. U. 1965 *J. Fluid Mech.* **22**, 217.

Cornish, R. J. 1928 *Proc. Roy. Soc.* A **120**, 691.

Davis, S. J. & White, C. M. 1928 *Proc. Roy. Soc.* A **119**, 92.

Gill, A. E. 1965 *J. Fluid Mech.* **21**, 145.

Kao, T. W. & Park, C. 1967 *Tech. Rep.* 67–032, *Dept. of Space Science and Applied Physics, The Catholic Univ. of America.*

Klebanoff, P. S. & Tidstrom, K. D. 1959 *NASA Tech. Note* no. D-195.

Klebanoff, P. S., Tidstrom, K. D. & Sargent, L. M. 1962 *J. Fluid Mech.* **12**, 1.

Leite, R. J. 1959 *J. Fluid Mech.* **5**, 81.

Lin, C. C. 1955 *The Theory of Hydrodynamic Stability.* Cambridge University Press.

Reynolds, W. C. & Potter, M. C. 1967 *J. Fluid Mech.* **27**, 465.

Schiller, L. 1923 *Z. angew Math. Mech.* **3**, 11.

Schubauer, G. B. & Skramstad, H. K. 1948 *NACA Tech. Rep.* no. 909.